Journal of Applied Polymer Science

A Physical Route to Porous Ethyl Cellulose Microspheres Loaded with TiO_2 Nanoparticles

Weiwei Cai, Hui Yang, Daxin Han, Xingzhong Guo
Department of Materials Science and Engineering of Zhejiang University, 38 Zheda Road, Xihu District, Hangzhou 310027, People's Republic of China
Correspondence to: X. Guo (E-mail: msewj01@zju.edu.cn)

ABSTRACT: Porous ethyl cellulose (EC) microspheres were prepared via a physical method in oil-in-water (O/W) emulsions. The morphologies and pore structures of the resulting porous microspheres were investigated by scanning electron microscopy (SEM), mercury porosimeter and spectrometer equipped with an integrating sphere. The increase of EC amount in oil phase will increase the size of the microspheres. All the microspheres possess open macropores in the shell and interconnected pores inside the microspheres by means of phase separation. The saturation of the Ethyl acetate (EA) in external phase has an effect on the morphology of the EC particles obtained. Using EA unsaturated aqueous solution as the external water phase in the emulsion process results in the formation of porous EC particles with irregular shape. The loaded TiO_2 nanoparticles uniformly disperse in EC matrix, and slightly deceases the size and volume of interconnected pores inside the microspheres. The addition of TiO_2 nanoparticles is also proved to increase the light-scattering power of the porous EC microspheres. © 2014 Wiley Periodicals, Inc. J. Appl. Polym. Sci. **2014**, *131*, 40822.

KEYWORDS: drug delivery systems; light scattering; optical properties; porous materials; synthesis and processing

Received 7 January 2014; accepted 6 April 2014
DOI: 10.1002/app.40822

INTRODUCTION

Increasing attention has been attracted by hollow microspheres due to their special characteristics, such as low density, low thermal conductivity, high specific surface, and good flow ability. Hollow microspheres have been widely used in all kinds of applications such as catalysis, adsorption, drug delivery and building materials.[1] Up to now, diverse porous microspheres with different special characteristics including hollow spheres with a single cavity,[2,3] hollow spheres with multiple shells,[4,5] and hollow sphere with multicavities,[6,7] have been fabricated by templating method, emulsion processing, high temperature treatment, layer-by-layer self-assembly technique, and so on. Wherein, hollow spheres with multicavities as an important class of hollow sphere have gained growing attention for their potential applications such as adsorption and catalysis, especially in drug delivery systems.[8–10] Moreover, the microspheres loaded with nanoparticles have been also fabricated for multiple applications, such as light diffusers[11] and magnetic-assisted separation agents.[12]

The rutile TiO_2 possesses strong light-scattering power when dispersed in resin, due to its high refractive index[13] (2.6–2.9, depending on the crystal axis). It has been reported that the TiO_2 particles will got even better light-scattering performance when dispersed in air. The introduction of the TiO_2 particles in the hollow microsphere containing dispersed microvoids will greatly increase the light-scattering power of the hollow microspheres.[14]

In this work, we demonstrate a physical method to synthesize porous ethyl cellulose (EC) microspheres loaded with TiO_2 nanoparticles (TNPs) in oil-in-water (O/W) emulsion. No templates were used, thus no extra treatment would be adopted to remove the residual the template. We investigate the effects of the mass ratio of ethyl cellulose (EC)/ethyl acetate (EA) in oil phase, unsaturated external water phase and TNPs content on the morphologies and pore structures of the porous microspheres. We also characterize the enhanced light-scattering power by means of the transmittance of the resin films containing EC microspheres and EC microspheres loaded with TNPs. It is also anticipated that the route presented in this work will offer a solution to fabricate organic porous microspheres with macropores in their shell and porous products loaded with functional nanoparticles.

EXPERIMENTAL

Materials

Ethyl cellulose (EC, CP, the degree of substitution of EC is 47%–48%), titanium dioxide nanoparticles (TNPs, rutile, ~100 nm, oleophylic) were purchased from Aladdin Reagent Co. Ltd. Ethyl acetate (EA, AR) and sodium dodecyl sulfate (SDS, CP)

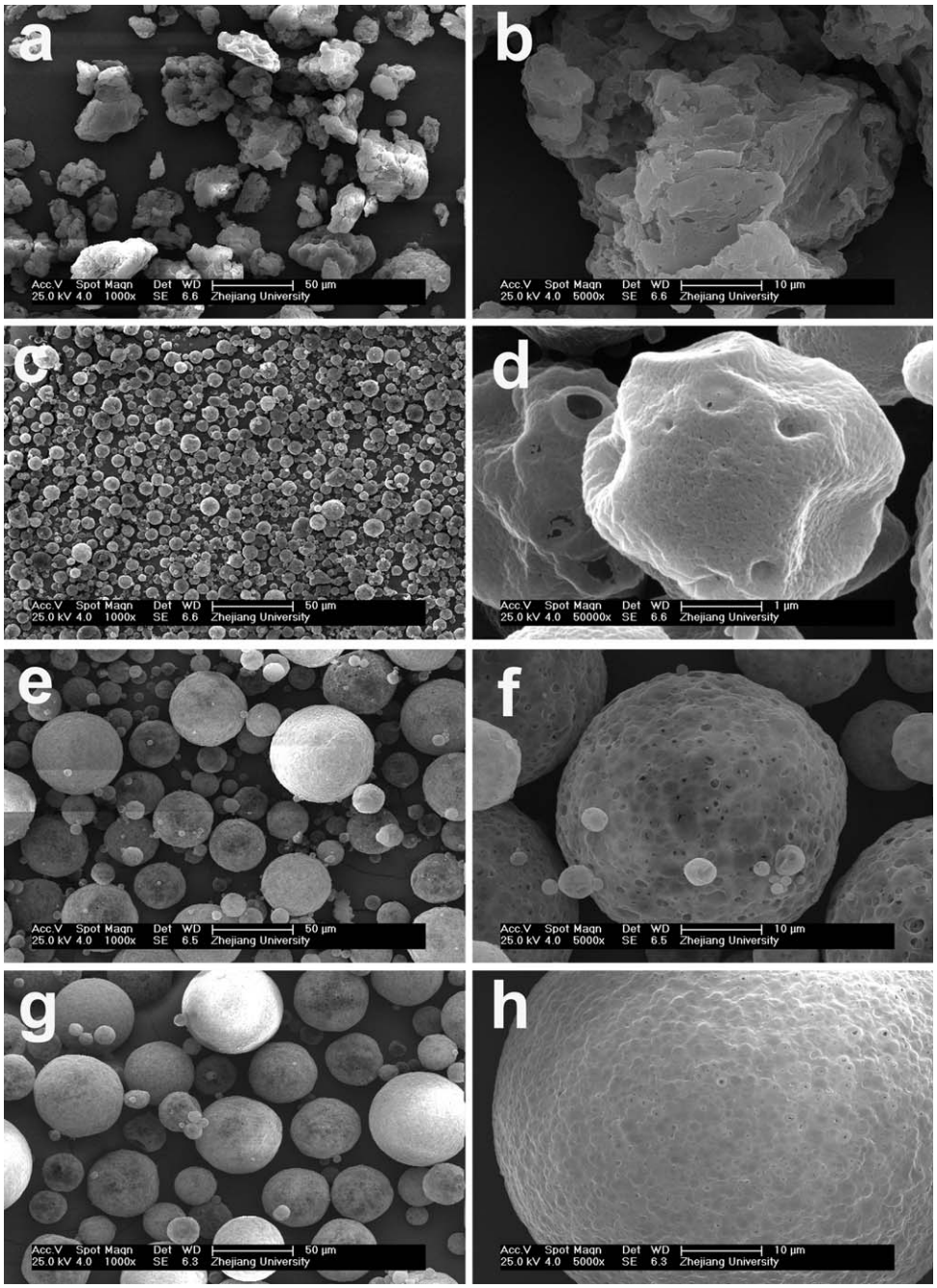

Figure 1. SEM images of EC microspheres prepared with different EC/EA mass ratios; (a and b) original particles, (c and d) 0.4 g EC/ 10 g EA, (e and f) 0.8/10, (g and h) 1.2/10; the insets: high-magnification SEM images of the EC particles.

were purchased from Sinopharm Chemical Reagent Co. Ltd. All the chemicals were used as received. The deionized water used was in Grade 3 (ISO 3696-1987).

Synthesization

Preparation of EA Saturated Aqueous Solution. A certain amount of deionized water was mixed with excessive amount of EA. The mixture was poured into a separatory funnel. And then, the separatory funnel with the mixture should be shaken several times and stood for 24 h at 20°C. The EA saturated aqueous solution can be obtained in the subnatant.

Synthesis of EC Microspheres. ***Emulsification.*** Firstly, an external water phase was prepared by mixing 2.0 g SDS with 100 g EA saturated aqueous solution. A selected amount (0.4, 0.8 and 1.2 g) of EC was added to 10.0 g EA with constant stirring for 1 h to prepare a clear solution as the oil phase. A certain amount (0.1, 0.2, and 0.4 g) of TNPs was added to oil phase under stirring for 1 h, and further homogenization was attained

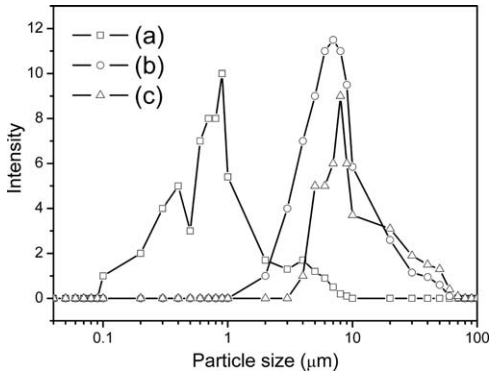

Figure 2. Particle size distributions of EC microspheres prepared with different EC/EA mass ratios; (a) 0.4 g EC/ 10 g EA, (b) 0.8 g EC/10 g EA, (c) 1.2 g EC/10 g EA.

by ultrasonic dispersion for 15 min. Secondly, the oil phase was added to the external water phase in one batch under stirring at 1000 rpm to obtain emulsion.

Solvent diffusion. After stirring for 1 h, the obtained emulsion was poured into the SDS aqueous solution obtained by mixing 1 g SDS and 300 g deionized water under stirring at 1000 rpm to induce solidification of the oil phase. After stirring for 1 h, the samples were collected by vacuum filtration and dried at 40°C for 24 h.

Preparation of the Films Containing EC Porous Microspheres. EC porous microspheres were mixed with a self-made acrylic varnish in various pigment concentrations. The blend of EC porous microspheres and acrylic varnish was coated over a glass slide using an applicator to give a nominal wet film thickness of 500 μm. The wet films were dried at room temperature for 24 h.

Characterization. The morphologies and size distributions of the microspheres were performed by using scanning electronic microscope (SEM, FEI Siron100). The morphology of the O/W emulsion after emulsification was observed by optical microscopy (CVM-600E, Chfang, China). The internal structure of the microspheres was revealed by cross-sectioning the microspheres embedded in a polyacrylate resin. The size distributions of pores inside the microspheres, the skeletal densities (ρ_s) and the apparent densities (ρ_a) of the microspheres were measured by a mercury porosimeter (AutoPore IV 9510, Micromeritics Co., USA) and the interconnected porosities (ε_i) can be calculated from ρ_s and ρ_a by means of the following equation:

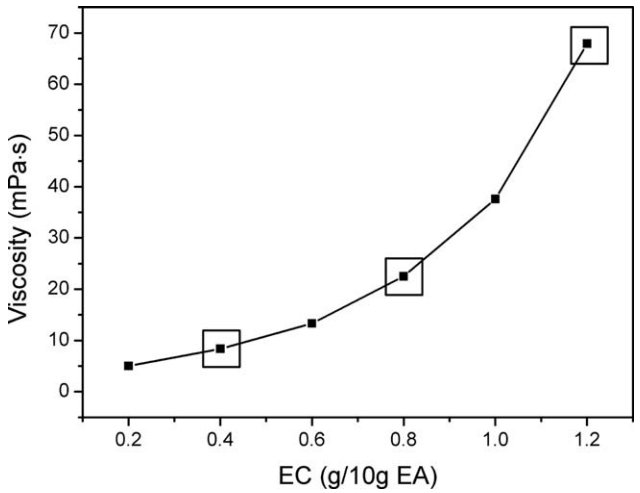

Figure 3. The viscosities of the oil phase with different EC/EA mass ratios.

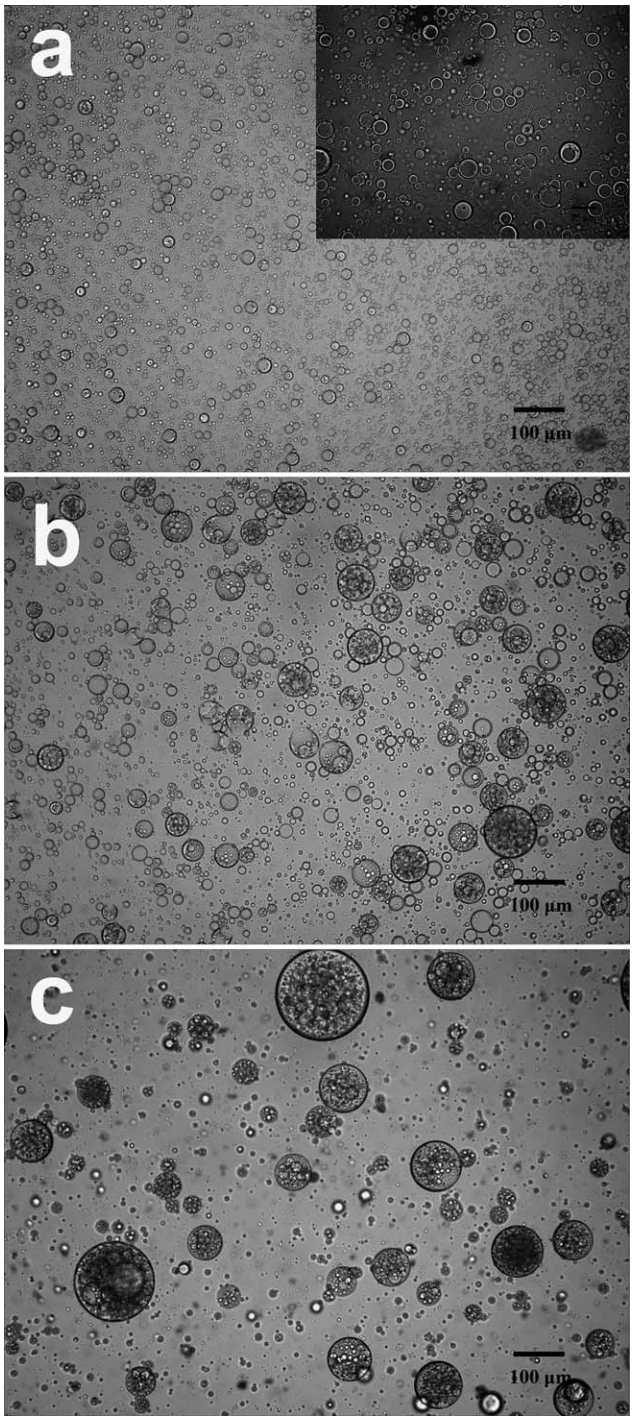

Figure 4. Optical microscope images of O/W emulsion prepared by oil phases with different EC/EA mass ratios; (a and b) 0.4 g EC/ 10 g EA, (c) 0.8 g EC/10 g EA, (d) 1.2 g EC/10 g EA.

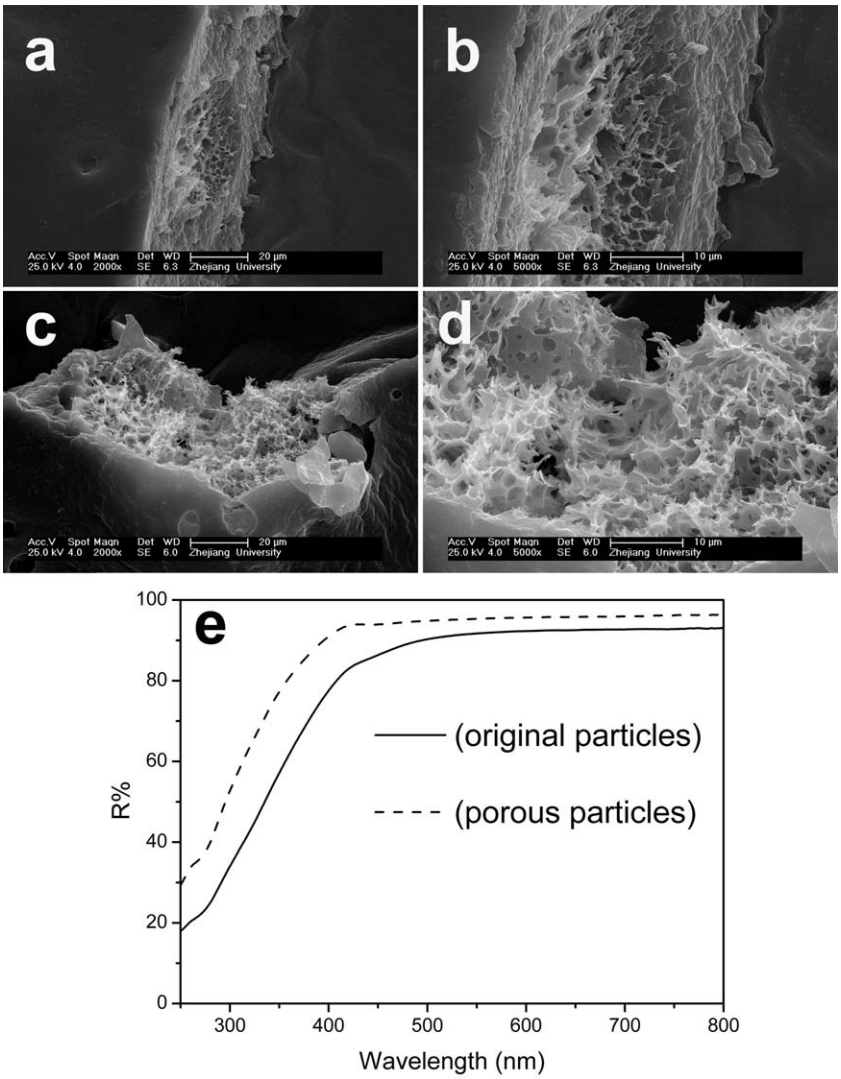

Figure 5. Cross-section of the EC microspheres prepared with EC/EA mass ratio=0.8/10 (a, b, c, and d) and the diffuse reflection spectra of the original particles and microspheres prepared with EC/EA mass ratio = 0.8/10 (e).

$$\varepsilon_i = \rho_a / \rho_s \quad (1)$$

Diffuse reflection UV–Visible spectra were obtained with a SHIMADZU UV-3150 spectrometer equipped with an integrating sphere. The viscometer (DV-II + Pro, Brookfield, USA) was used to measure the viscosities of the oil phase consisting of EC and EA. Thermogravimetric (TG) analysis of the microspheres loaded with TNPs was carried out by using a TG-DTA analyzer (German Netzsch Co. STA449C) at a heating rate of 10°C/min, and the final TNPs/EC mass ratio of obtained microspheres were calculated accordingly. The transmittance of the films containing EC porous microspheres was performed by spectrum transmission meter (LS 102, Linshang, China).

RESULTS AND DISCUSSION

During the preparation, the oil phase was firstly mixed with the external water phase saturated by EA and broken into small droplets by high-speed shearing. When the obtained emulsion was subsequently poured into the water without EA, the EA began to diffuse outwards and dissolute into the water and finally resulted in a solid microsphere. Figure 1 shows the SEM images of original EC particles and EC microspheres prepared with different EC/EA mass ratios. Apparently, the original particles of EC have no specific morphologies, while three particles obtained via the physical method are spherical. The size distributions of the three EC microspheres derived from the SEM images are shown in Figure 2. The size of the resulting microspheres enlarges with increasing EC/EA mass ratio. The average sizes of EC microspheres obtained with 0.4/10 of EC/EA mass ratio, 0.8/10 of EC/EA mass ratio and 1.2/10 of EC/EA mass ratio are 2.6, 15.7, and 23.1 μm, respectively.

Figure 3 shows the viscosities of the oil phase with different EC/EA mass ratios. The viscosities of the oil phase increases with increasing additive EC. Generally, the heightened viscosity imparts the stability against breakup of the droplets by increasing the rigidity of the droplet/water interface, which results in an increased steady-state drop size.[15,16] Thus the increased size of obtained microspheres can be attributed to the increase of

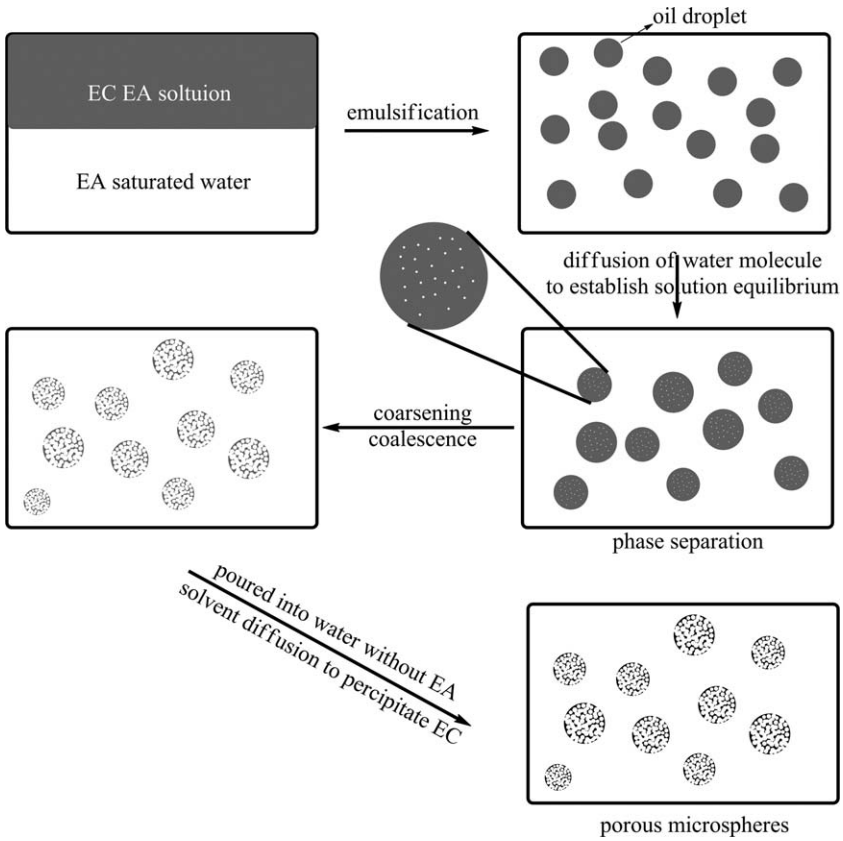

Figure 6. Illustrative mechanism for the formation of porous EC microspheres.

viscosity of the dispersed phase, which results from increasing the additive EC in oil phase. The effect of heightened viscosity on the size of droplets can also be illustrated in Figure 4, which shows the optical microscope images of O/W emulsion prepared by oil phases with different EC/EA mass ratios. It is seen that the size of oil droplets in the emulsions generally increases with increasing EC/EA mass ratio. And when the obtained emulsion is poured into the SDS aqueous solution, the dissolution of EA into water phase induces a rigid shell on initial stage of dissolution, which dramatically suppresses both breakup and coalescence of dispersed droplets. Also, as shown in Figure 4, spherical structures with new boundaries form within the oil droplets. As it is well known, EA and water is partially miscible. Thus, as there is no additive water in the oil phase, the water molecule of the external phase can diffuse into the oil phase to establish solubility equilibrium between the external phase and the oil phase. The diffused water in oil phase will initiate phase separation due to the immiscibility between water and EC. As a result, the system is separated into EC-rich (water-poor) phase and EC-poor (water-rich) phase, and the EC-poor phase is entrapped in the EC-rich phase to form the spherical structures within the oil droplets. The separated phases will also undergo coarsening and coalescence to reduce interfacial free energy.

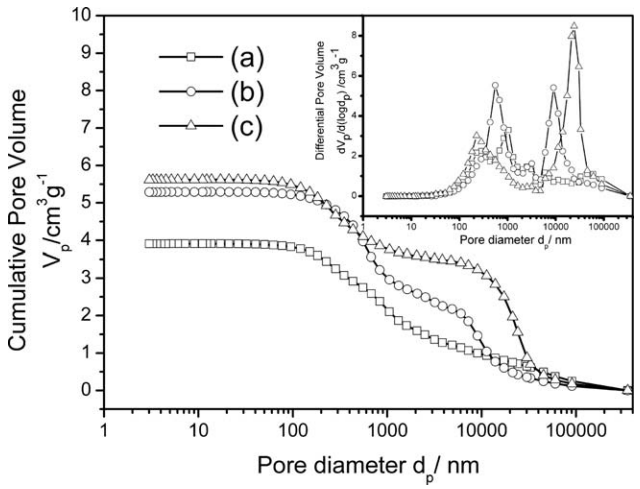

Figure 7. Macropore size distributions of the EC microspheres prepared with different EC/EA mass ratios; (a) 0.4 g EC/10 g EA, (b) 0.8 g EC/10 g EA, (c) 1.2 g EC/10 g EA.

Figure 5 shows the cross-section of the EC microspheres prepared with 0.8/10 of EC/EA mass ratio. The cross-sectional views show that there are a lot of interconnected pores inside the microspheres. In addition, as reported previously,[17,18] the incorporated microcavities into the matrices could enhance the reflectance properties which can be closely related to Mie scattering. Thus, the diffuse reflecting performance of the EC particles was characterized. The resulting spectra in Figure 5(e) show that the porous EC microspheres attain higher diffuse reflectance than that of original particles in 250–800 nm wavelength region, which further confirms the porous structure.

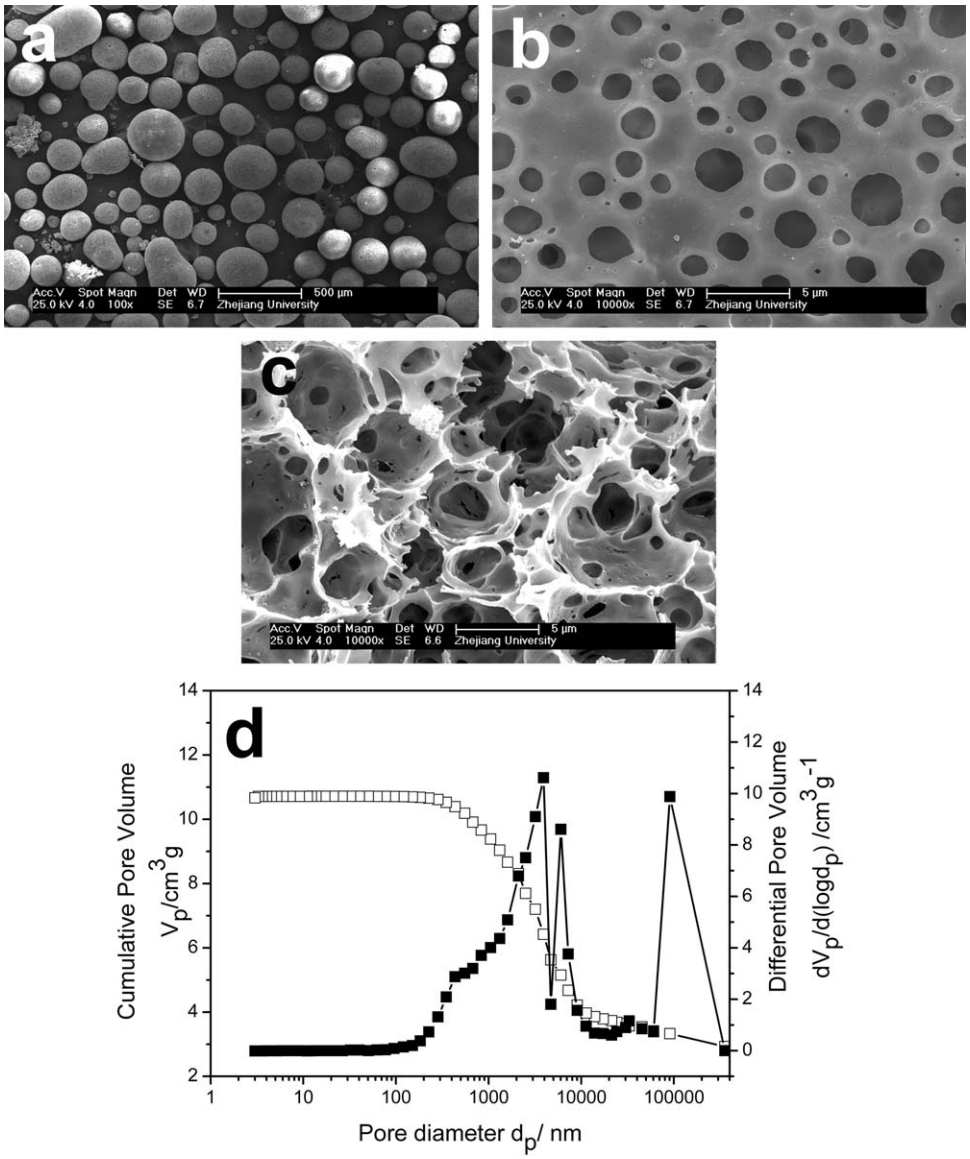

Figure 8. The SEM images of the EC microspheres prepared with EA half-saturated aqueous solution (a, b, and c) and the macropore size distribution (d).

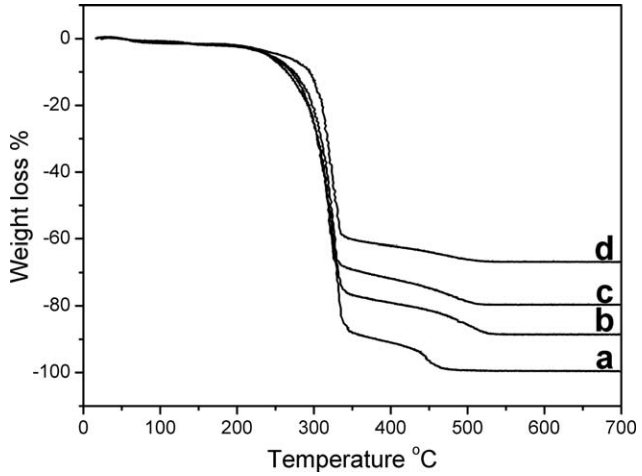

Figure 9. The TG curves of the EC porous microspheres loaded with different TNPs contents; (a) 0 g TNPs/0.8 g EC, (b) 0.1/0.8, (c) 0.2/0.8, (d)0.4/0.8.

As mentioned, during the process of emulsification, spherical structures were formed within the oil droplets due to phase separation. And during solvent diffusion, EA in oil droplets began to dissolve into external water phase and the EC were gradually precipitated in the oil droplets to make a solid microspheres, which also means a dramatically enhanced viscosity of oil droplets.[19,20] Thus the final porous structure of obtained microspheres after solvent diffusion may be derived from the spherical structure formed inside the oil droplets, while the interconnected structure of the pores inside the microspheres is possibly attributed to partially coalescence of the spherical structure formed inside the oil droplets which were finally maintained by dramatically enhanced viscosity. In addition, as illustrated in SEM images (Figure 1), all the obtained microspheres have open macropores in their shells, and it can be attributed to the eruption of EC-poor phase entrapped inside

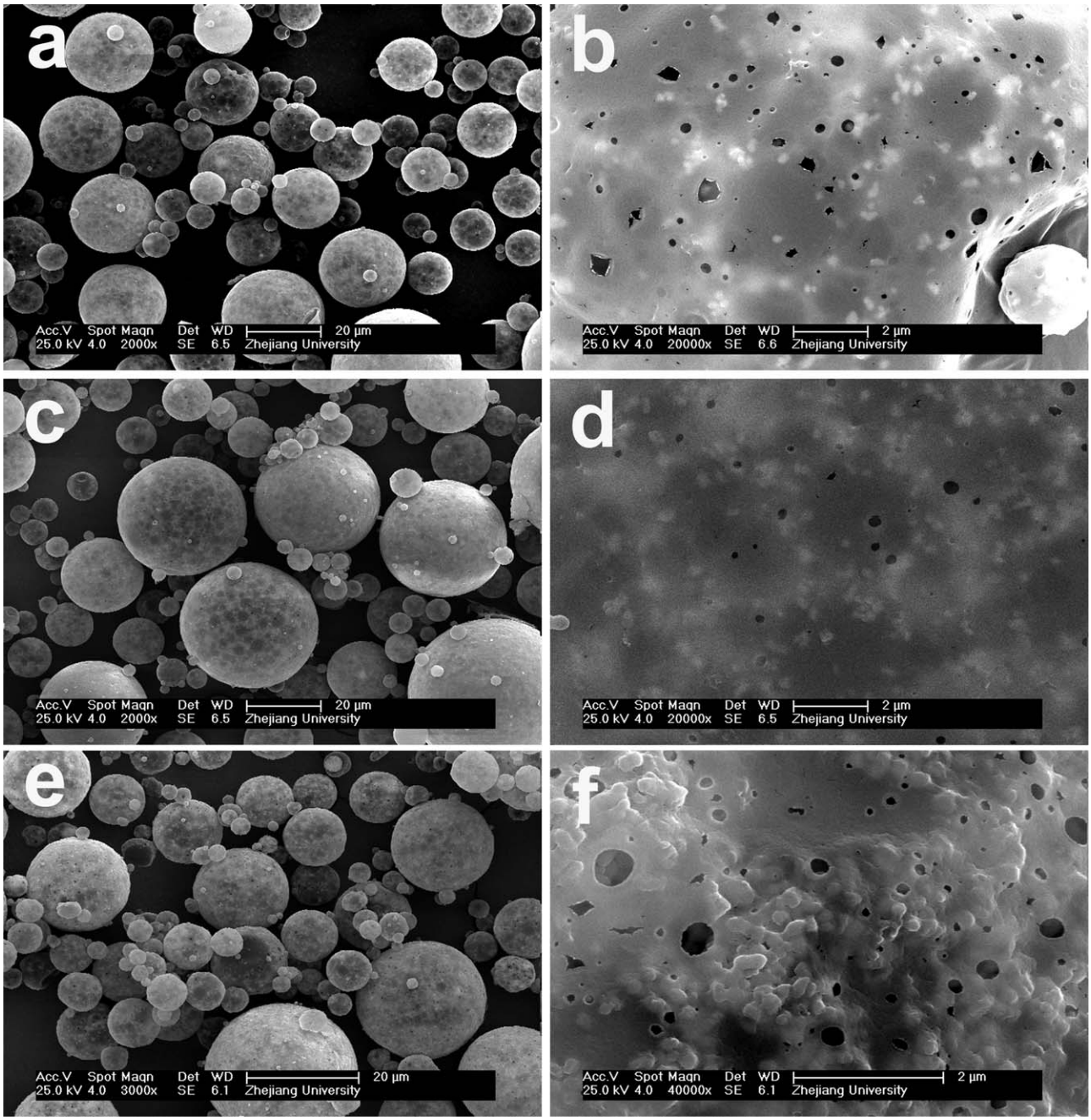

Figure 10. The SEM images of EC spherical loaded with different TNPs contents; (a and b) 0.1 g, (c and d) 0.2 g, (e and f) 0.4 g.

the droplets. The dissolution of EA in water leads to the contraction of the oil droplets because of decreased mass and increased density. Therefore, the EC-poor phase entrapped inside is compressed within the oil droplets. The contraction induced by dissolution of EA increases the pressure of liquid EC-poor phase inside. And, finally the liquid EC-poor phase bursts, which leads to the formation of open macropores in the shells.[12] The illustrative mechanism for the formation of porous EC microspheres is shown in Figure 6.

In order to further confirm the pore structures inside the microspheres and the effect of increasing the additive EC in oil phase, the pore size distributions of the three microspheres were characterized by Hg porosimetry. Figure 7 shows the macropore size distributions of the EC microspheres with different EC/EA mass ratios. The mercury was first pumped into the pores among the particles and then increasing pressure facilitated the mercury into the inner space of the particles.[21] Thus, the distribution curve of the spherical microspheres shows typical bimodal distribution. Generally, the sizes of the pores among the particles are larger than that of the inner cavities. As shown in the distribution curves, the diameter of the pores among the particles increases with the EC/EA mass ratio. This also indicates that the size of the

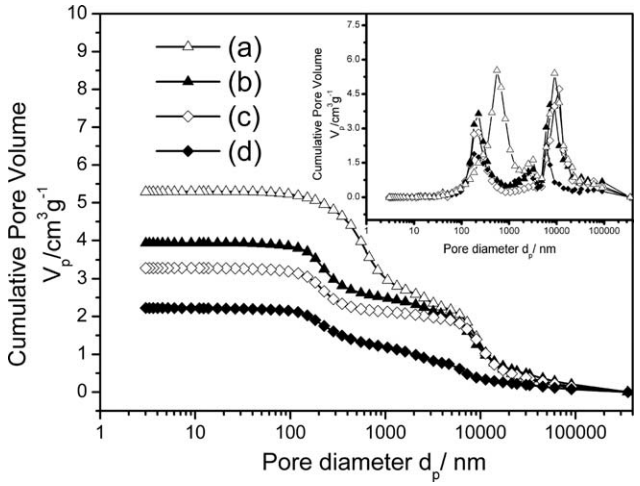

Figure 11. Pore size distributions of the spherical EC microspheres prepared with different TNPs contents; (a) 0 g TNPs/0.8 g EC, (b) 0.1/0.8, (c) 0.2/0.8, (d)0.4/0.8.

microspheres increases with increasing additive EC, which consists with the observation of SEM images (Figure 1). In addition, the size distribution of the inner pores shows large cumulative pore volume for all the three microspheres. The interconnected porosities calculated for the three spherical samples are 72%, 74%, and 68%, respectively. This implies the existence of large amounts of interconnected pores inside the microspheres, which coincides with the observation of the cross-sectional views of the microspheres.

The effect of the saturation of the EA in external phase on the morphology of the EC particles obtained was also investigated. During the process of preparation, the EA saturated aqueous solution was diluted with deionized water of the same volume to fabricate the external phase (EA half-saturated aqueous solution). The morphology and the cross-section of the fabricated particle and its cavity size distribution are shown in Figure 8. As shown by the SEM image of

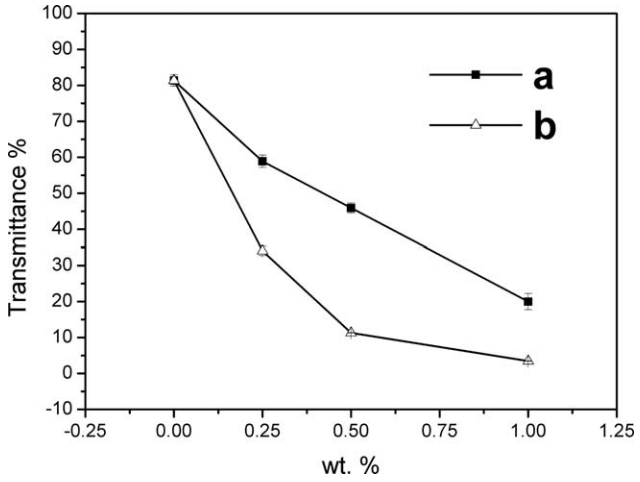

Figure 12. The transmittance of the films with porous EC microspheres (a) and porous EC microspheres loaded with TNPs (b) in 200–380, 380–760, and 760–2500 nm wavelength regions, respectively; (a) 0.8 g EC/10 g EA, (b) 0.2 g TNPs/0.8 g EC/10 g EA.

the obtained particles [Figure 8(a)], the obtained particles attain irregular shape with size distribution of 100–500 μm. Due to the unsaturated water phase, the dissolution of EA begins at the initial stage of emulsion process to enhance the viscosity and subsequently induces a rigid shell against shearing breakup. Also, the diffusion of the water molecules into the oil droplets can also induce the phase separation, which results in the porous structures. The irregular shape can be the result of deformation of oil droplets induced by high-speed shearing and sequent solidification of the shell at the initial stage of emulsion process. Also, the resulting particles have open macropores in the shell as shown in Figure 8(b). The cross-sectional view in Figure 8(c) shows that the obtained particles are porous and the pores inside are generally interconnected. As mentioned, the open macropores in the shell can be attributed to the eruption of EC-poor phase entrapped inside the droplets and the porous structure is attributed to phase separation. However, the pore size distribution of the particles in Figure 8(d) shows that the microspheres prepared with unsaturated external water phase attain larger pore size than that of the microspheres with saturated external water phase. It might be suggested that the enlarged size of the droplets can suppress the diffusion of water to establish solubility equilibrium due to the decreased specific surface area and provide more time for coarsening and coalescence before poured into pure water for further solidification. Thus, it can be concluded that the saturation of EA in external water phase surely has great effect on the morphologies and internal structures of the obtained particles.

The EC microspheres loaded with 0.1, 0.2, and 0.4 g TNPs were also prepared via this route, respectively. Figure 9 shows the TG curves of the EC porous microspheres loaded with different TNPs contents. As shown in Figure 9, the weight loss generally begins at the temperature of 200°C, which can be attributed to the decomposition of EC matrix, and the weight loss between the temperature of 350 and 500°C can be attributed to the decomposition of remaining organics. According to the TG analysis, the final loadings of TNPs in EC microspheres (TNPs/EC mass ratio) were caculated. The TNPs/EC mass ratio caculated from the TG curves are 12.7%, 25.5%, and 49.6%, respectively, while the TNPs/EC mass ratios are 12.5%, 25.0%, and 50.0% when preparing EC porous microspheres loaded with TNPs. It indcates that almost all the additive TNPs are entrapped in the obtained microspheres.

Figure 10 shows the SEM images of microspheres with different TNPs contents. When the TNPs content is 0.1 or 0.2 g, the TNPs disperse uniformly in the EC, and only have a little agglomeration. When the TNPs content reaches to 0.4 g, the agglomeration of TNPs further develops to form a rough surface morphology, as shown in Figure 10(f). It is also seen that the addition of TNPs has little effect on the size of the open pores in the shell, while the additive TNPs has an obvious effect on the interconnected pores inside the microspheres, as shown in Figure 11. The size of interconnected pores decreases with the addition of TNPs, while a continuous increase in the

TNPs content has little effect on the interconnected pore size. The addition of TNPs might restrain the coalescence of the separated domain during the cavity-forming process to induce smaller cavity sizes. In addition, four skeletal densities obtained from Hg porosimetry are 0.94, 0.85, 0.95 and 1.02 g/mL, respectively. As we know, the TNPs (~4 g/mL) attain much higher density than that of EC (~1 g/mL), and the additive TNPs will increase the apparent density. Thus the decreased apparent density (0.85 g/mL) after the addition of 0.1 g TNPs might be attributed to increased closed pores which cannot be filled by Hg, while the subsequent increase of the apparent density can be attributed to the increase additive TNPs from 0.1 to 0.4 g. The increased closed pores also might be attributed to the restrained coalescence induced by additive TNPs. In addition, the interconnected porosities calculated from the results of Hg porosimetry are approximately 74%, 56%, 54%, and 51% for four samples, respectively, which further demonstrates that the formation of the interconnected pore is restrained by adding TNPs.

The hiding power of the particles is generally related to their light-scattering power,[22] thus the transmittance of resin films containing particles is also related to the light-scattering power of the particles. Therefore, in order to confirm the effect of loaded TNPs on the scattering power of EC porous microspheres, EC microspheres are blend with acrylic resin to make films and the measurement of transmittances of obtained films are taken. Figure 12 shows the transmittance of the films prepared with porous EC microspheres (a) and porous EC microspheres loaded with TNPs. The transmittance of films generally decreases with increasing additive EC microspheres. And after loaded with TNPs, the EC microspheres increases the performances in hindering the transmission of incident light in 380–760 nm wavelength regions, which indicates an increase in the scattering power for incident light.

CONCLUSIONS

The porous EC microspheres loaded with TNPs were successfully prepared in oil/water (O/W) emulsion. All the obtained spherical samples possessed open macropores in the shell and interconnected pores inside the microspheres. And the enlarged size of EC microspheres could be obtained by increasing EC/EA mass ratio from 0.4/10 to 1.2/10. The interconnected porosities of the samples obtained with 0.4/10, 0.8/10 and 1.2/10 of EC/EA mass ratio were 72%, 74%, and 68%, respectively. The large anomalous spherical porous particles with size distribution of 100–500 μm and open macropores in the shells were obtained. The addition of TNPs decreased the interconnected porosity of the microspheres and the size of interconnected pores, while a continuous increase in the TiO_2 nanoparticles amount from 0.1 g to 0.4 g had little effect on the size of interconnected pores. The loading of the TNPs improved the light-scattering power of EC porous microspheres. The route presented in this work will offer an anticipated approach to fabricate organic porous microspheres loaded with inorganic functional nanoparticles.

ACKNOWLEDGMENTS

This work is supported by the National Natural Science Foundation of China (51372225) and Zhejiang Provincial Natural Science Foundation of China (LY13B010001).

REFERENCES

1. Hu, J.; Chen, M.; Fang, X. S.; Wu, L. M. *Chem. Soc. Rev.* **2011**, *40*, 5472.
2. Schacht, S.; Huo, Q.; Voigt-Martin, I. G.; Stucky, G.D.; Schüth, F.; *Science* **1996**, *273*, 768.
3. Nakashima, T.; Kimizuka, N. *J. Am. Chem. Soc.* **2003**, *125*, 6386.
4. Xu, H. L.; Wang, W. Z. *Angew. Chem. Int. Ed.* **2007**, *46*, 1489.
5. Guan, J. G.; Mou, F. Z.; Sun, Z. G.; Shi, W. D. *Chem. Commun.* **2010**, *46*, 6605.
6. Lee, S. J.; Park, J. K. *Ceram. Int.* **2003**, *29*, 271.
7. Wang, M. Z.; Wang, H.; Ge, X. W. *Polymer* **2008**, *49*, 4974.
8. Han, J.; Fang, P.; Dai, J.; Guo, R. *Langmuir* **2012**, *28*, 6468.
9. Xu, J. X.; Chen, G. J.; Yan, R.; Wang, D.; Zhang, M. C.; Zhang, W. Q.; Sun, P. C. *Macromolecules* **2011**, *44*, 3730.
10. Kamio, E.; Yonemura, S.; Ono, T.; Yoshizawa, H. *Langmuir* **2008**, *24*, 13287.
11. Kim, S. H.; Cho, Y. S.; Eun, T. H.; Yi, G. R.; Yang, S. M. *Adv. Mater.* **2008**, *20*, 3268.
12. Li, L.; Choo, E. S.; Tang, X.; Ding, J.; Xue, J. *Chem. Commun.* **2009**, *45*, 938.
13. Nussbaumer, R. J.; Caseri, W. R.; Smith, P.; Tervoort, T. *Macromol. Mater. Eng.* **2003**, *288*, 44.
14. Ross, W. D.; *Ind. Eng. Chem., Prod Res. Develop.* **1974**, *13*, 45.
15. Dowding, P. J.; Vincent, B. *Colloids Surf., A* **2000**, *161*, 259.
16. Jahanzad, F.; Sajjadi, S.; Brooks, B. W. *Ind. Eng. Chem. Res.* **2005**, *44*, 4112.
17. Seiner, A. J. *Ind. Eng. Chem. Prod. Res. Dev.* **1978**, *17*, 302.
18. Fujiwara, M.; Shiokawa, K.; Sakakura, I.; Nakahara, Y.; *Langmuir* **2010**, *26*, 6561.
19. Nakanishi, K.; *J. Porous Mater.* **1994**, *4*, 67.
20. Hindmarsh, J. P.; Su, J. H.; Flanagan, J.; Singh, H.; *Langmuir* **2005**, *21*, 9076.
21. Nair, M.; Lusignan, C. P.; Boris, D. C.; *Colloids Surf., A* **2014**, *443*, 583.
22. Park, J. M.; Hong, S. M.; *J. Ind. Eng. Chem.* **2001**, *7*, 23.